

# Microstructure of $MmM_5/Mg$ Multi-Layer Hydrogen Storage Films Prepared by Magnetron Sputtering

L.Z. OUYANG,<sup>1</sup> H. WANG,<sup>1</sup> M. ZHU,<sup>1\*</sup> J. ZOU,<sup>2</sup> AND C.Y. CHUNG<sup>3</sup>

<sup>1</sup>College of Mechanical Engineering, South China University of Technology, Guangzhou, 510641, People's Republic of China

<sup>2</sup>Division of Materials and Centre for Microscopy and Microanalysis, The University of Queensland, QLD 4072, Australia

<sup>3</sup>Department of Physics and Material Science, City University of Hong Kong, Kowloon, Hong Kong

**KEY WORDS** transmission electron microscopy; hydrogen storage alloys; thin films; magnetron sputtering

**ABSTRACT** Multi-layer hydrogen storage thin films with Mg and  $MmNi_{3.5}(CoAlMn)_{1.5}$  (here Mm denotes La-rich mischmetal) as alternative layers were prepared by direct current magnetron sputtering. Transmission electron microscopy investigation shows that the microstructure of the  $MmNi_{3.5}(CoAlMn)_{1.5}$  and Mg layers are significantly different although their deposition conditions are the same. The  $MmNi_{3.5}(CoAlMn)_{1.5}$  layer is composed of two regions: one is an amorphous region approximately 4 nm thick at the bottom of the layer and the other is a nanocrystalline region on top of the amorphous region. The Mg layer is also composed of two regions: one is a randomly orientated nanocrystalline region 50 nm thick at the bottom of the layer and the other is a columnar crystallite region on top of the nanocrystalline region. These Mg columnar crystallites have their [001] directions parallel to the growth direction and the average lateral size of these columnar crystallites is about 100 nm. A growth mechanism of the multi-layer thin films is discussed based on the experiment results. *Microsc. Res. Tech.* 64:323–329, 2004. © 2004 Wiley-Liss, Inc.

## INTRODUCTION

In the past several decades, tremendous effort has been made to develop hydrogen storage alloys since these may play key roles in clean energy systems. Among the major hydrogen storage alloys developed so far, Mg-based alloys have been considered as candidates with significant potential for their high hydrogen storage capacity (up to 7.6 mass%). However, hydrogenation and dehydrogenation kinetics of Mg-based alloys are poor and a high reaction temperature (~573 K) is generally required. In order to overcome these drawbacks, different methods, such as alloying element addition (Bobet et al., 2000a,b, 2001; Cui et al., 1999; Yamaura et al., 2002; Zaluska et al., 2001), mechanical alloying (MA) (Cui et al., 1999; Zhu et al., 2003), surface modification (Yang et al., 1998), and forming non-equilibrium microstructure including nanocrystalline and amorphous (Huot et al., 2003; Nohara et al., 1998; Orimo and Fujii, 2001) have been applied.

With respect to the non-equilibrium structured Mg-based alloys, MA has mainly been applied to synthesize them. Many previous works (Aizawa et al., 1999; Berlouis et al., 2000; Hong et al., 2000; Lee et al., 2000) show that the properties of Mg-based hydrogen storage alloys are improved owing to the fact that MA may induce amorphous and/or nanocrystalline structures. (Zhu et al., 2003). The kinetic properties of Mg-based alloys can be further improved by incorporating catalytic components in them to form nano-composites. For instances, Mg-Ni based alloys were mechanically ground with Zr (Goo et al., 2000),  $LaNi_5$  (Gap et al., 2003), FeTi (Morris et al., 1999), and  $TiV_{2.1}Ni_{0.3}$  (Choi et al., 2000) (graphite) Gr (Imamura and Sakasai, 1995; Kohno et al., 1999), and Ni (Imamura et al., 1996) to form nano-composites, and the hydrogen storage performance of the Mg-Ni based alloys was im-

proved. This method is also effective in improving the electrode properties, such as the cycle life and discharge capacity, of Mg-Ni based alloys (Choi et al., 2000; Gao et al., 2003; Morris et al., 1999).

Inspired by the work on MA of Mg-based alloys, film deposition techniques have also been used to synthesize non-equilibrium and composite Mg-based alloys in recent years (Higuchi et al., 2002; Richardson et al., 2003). Chen et al. (2002) reported that an amorphous  $Mg_{1.2}Ni_{1.0}$  film could absorb and desorb hydrogen under 3.3 MPa at 150°C. It was reported that the Pd/Mg/Pd films can absorb and desorb hydrogen at 100°C and its hydrogen storage capacity could reach to 5 mass% (Fujii and Orimo, 2003). Since the cost of Pd is high, alternative catalytic components, such as Ti and Ni, have been added to Mg-based films, and their effect on the kinetics has been studied (Chen et al., 2002; Pailier et al., 2003).

Although many Mg-based nanostructured composites prepared by the methods of MA and film deposition have been investigated, the correlation between their hydrogen storage properties and microstructure is still not very clear. In a recent work (Wang et al., 2004), we prepared  $MmNi_{3.5}(CoAlMn)_{1.5}/Mg$  ( $MmM_5$  denotes

\*Correspondence to: M. Zhu, College of Mechanical Engineering, South China University of Technology, Guangzhou, 510641, People's Republic of China. E-mail: memzhu@scut.edu.cn

Received 18 May 2004; accepted in revised form 14 August 2004

Contract grant sponsor: National Nature Science Foundation; Contract grant numbers: 59925102, 50131040; Contract grant sponsor: Ministry of Science and Technology; Contract grant number: 2002CCA02300; Contract grant sponsor: The Australian Research Council; Contract grant numbers: F89905431 and A00104346; Contract grant sponsor: Research Grants Council of the Hong Kong Special Administrative Region, China; Contract grant number: CityU 1316/03E.

DOI 10.1002/jemt.20089

Published online in Wiley InterScience (www.interscience.wiley.com).

MmNi<sub>3.5</sub>(CoAlMn)<sub>1.5</sub> below) multi-layer thin films that can absorb/desorb hydrogen at 245°C. However, their structural information is basically unknown. In this report, we investigated the microstructure of MmM<sub>5</sub>/Mg multi-layer thin films in detail by transmission electron microscopy (TEM) and high resolution transmission electron microscopy (HRTEM). Based on the obtained microstructures, detailed growth mechanisms of different layers are discussed.

## EXPERIMENTS

MmM<sub>5</sub>/Mg multi-layer thin films were deposited onto a (001) Si substrate by direct current (DC) magnetron sputtering using an Edwards Coating System (Model E306A). The Si substrate was pasted onto the substrate stage using a double-stick tape and the substrate stage was cooled by circulating water. Two sputtering targets were used with one being MmM<sub>5</sub> alloy prepared by induction melting under the protection of pure argon and the other being Mg ingot with a purity of 99.99%. The base pressure in the working chamber was  $5 \times 10^{-7}$  mbar and the working pressure in the chamber was maintained a constant value of  $1.4 \times 10^{-3}$  mbar during the deposition. The applied power was 250 W. The deposition rate was monitored by an Edwards FTM<sub>5</sub> thickness monitor calibrated using an Alpha-step<sup>®</sup> 500 Surface Profiler. In the deposition process, the MmM<sub>5</sub> and Mg targets were alternatively positioned below the substrate and sputtered to deposit the MmM<sub>5</sub> and Mg layers alternatively with designed thicknesses. Seven-layered films were deposited with the starting and finishing layer being MmM<sub>5</sub>.

Cross-section TEM (XTEM) specimens were prepared in the following manner: (1) the bulk sample was mechanically thinned from the back (substrate) side into a thin wafer containing the thin film/substrate; (2) the thin wafer was cleaved into several slices vertically; (3) several of these slices were glued together to form a block sample in a face-to-back fashion; (4) the block sample was mechanically thinned and polished from both sides into a wedged shape and mounted on a Cu slot grid; (5) the thin sample was further thinned to electron transparency using an ion beam in a Gatan precision ion polishing system. The structural and compositional investigation of XTEM specimens was carried out using a Philips CM12 TEM operated at 120 kV and a JEOL 3000F equipped with an energy dispersive X-ray spectrometer (EDX) and operated at 300 kV. The probe size of the electron beam for performing EDX analysis could be as small as 0.5 nm in diameter.

## RESULTS AND DISCUSSION

### General Morphology of the Thin Film

Figure 1 is a bright field XTEM image of a MmM<sub>5</sub>/Mg multi-layer thin film. It shows that the total film thickness is 3,100 nm with the Mg layers and the MmM<sub>5</sub> layers being 500 and 400 nm thick, respectively. The thickness of each layer was accurately controlled, and the thickness is homogeneous for the entire layers. The Mg layers and the MmM<sub>5</sub> layers are bonded well and the interfaces are sharp and clear. No other phases have been observed along the interface regions, implying that there was no reaction between Mg and MmM<sub>5</sub> during the deposition process. This is different to the MA of Mg and MmM<sub>5</sub>, where a solid-state reaction takes place between Mg and MmM<sub>5</sub> (Gao et al., 2003).

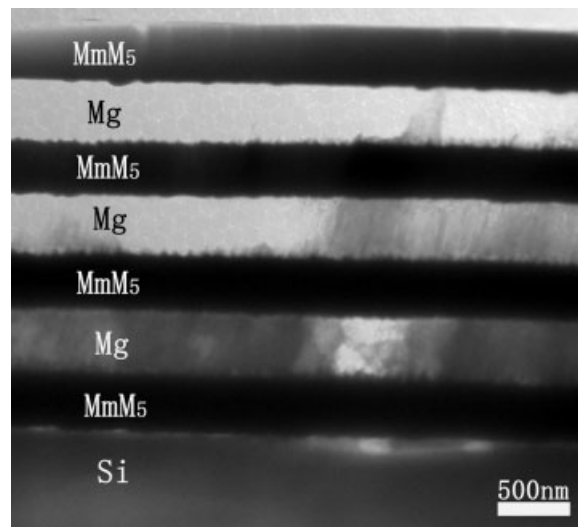


Fig. 1. XTEM image of a MmM<sub>5</sub>/Mg multi-layer thin film prepared by direct current magnetron sputtering on Si substrate.

However, detailed investigation indicated that the interfaces are not perfectly flat and small fluctuations exist along interfaces. Careful TEM and HRTEM observation show that the Mg layer and the MmM<sub>5</sub> layer have their own specific microstructural feature. The details of these microstructure features are described below individually.

### Microstructure of the MmM<sub>5</sub> Layer

It can be noted from Figure 1 that MmM<sub>5</sub> layers in the multi-layer thin film were grown on two different bases. One is on the single crystal (001) Si substrate and the other is on the as-deposited Mg layer. Figure 2a shows the interface region between an MmM<sub>5</sub> layer and the (001) Si substrate. Since Figure 2a was obtained with the [110] direction of Si being parallel to the electron beam, the interface between the Si and MmM<sub>5</sub> is at the edge-on position. As demonstrated in Figure 2a, a thin amorphous layer about 4 nm thick is formed on the Si substrate. EDX analysis of the thin amorphous layer proved that its composition is consistent with the MmM<sub>5</sub> alloy, meaning that the amorphous layer was formed in the initial deposition stage of the MmM<sub>5</sub> layer on the Si substrate. With further growth, the amorphous phase changes to a crystalline phase. The electron diffraction pattern taken from the crystalline region is inserted in the top-left corner of Figure 2a. Indexing of the electron diffraction pattern confirms that the crystalline phase has the CaCu<sub>5</sub> structure. The continuity of the diffraction halos reveals that the grain size of the crystalline phase is rather small. Grains have been estimated to be about 3–10 nm from HRTEM image. Our extensive TEM investigation confirms that, once the nanocrystalline grains are formed, the rest of the MmM<sub>5</sub> growth would keep this fashion to the end of the layer growth.

Figure 2b shows the interface region between an MmM<sub>5</sub> layer and an underlying Mg layer. With the imaging orientation of the specimen the same as that of Figure 2a, the interface is parallel to the electron beam. A similar morphology is observed as in the case of an

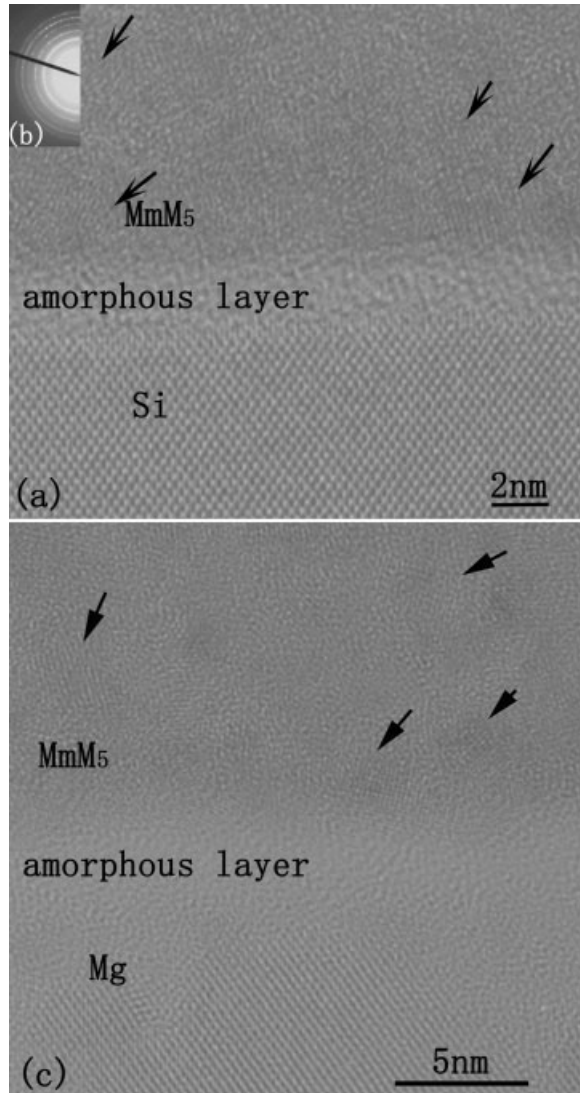


Fig. 2. HRTEM images of  $\text{MmM}_5$  layers deposited on (a) a Si substrate with a corresponding SADP inserted and (b) an underlying Mg layer, showing the amorphous and nanocrystalline regions.

$\text{MmM}_5$  layer deposited onto a Si substrate (as shown in Fig. 2a), that is, an amorphous layer of about 4 nm thick is found on the Mg layer and its composition, as confirmed by EDX, is consistent with the  $\text{MmM}_5$  alloy. The rest of this layer is nanocrystalline  $\text{MmM}_5$  phase. Overall, the  $\text{MmM}_5$  layers deposited onto the Si substrate and an underlying Mg layer are essentially the same from the microstructure point of view.

As reported in previous work (Wang et al., 2004), an amorphous phase is easily formed when  $\text{MmM}_5$ -base alloy is rapidly solidified. It is noted, in the present case, that the Si substrate was completely cold before the deposition process because the substrate was cooled by circulating water throughout the deposition process. As a result, the deposited material should experience a rapid cooling and consequently form an amorphous layer at the initial stage of the deposition of the  $\text{MmM}_5$  film. With further growth of the  $\text{MmM}_5$  film, the substrate was warmed up due to the non-steady

state thermal processing condition and the initially formed amorphous layer also acted as a thermal barrier to the substrate cooling. Therefore, the formation of the crystalline  $\text{MmM}_5$  phase could not be suppressed and crystalline  $\text{MmM}_5$  nuclei are formed on the surface of the amorphous layer. A similar result has been reported by Zhou et al. (2003). Since the cooling rate in the deposition process is rather high, the nucleation rate of the crystalline phase is high and its growth rate is low. Furthermore, the complicated composition of the  $\text{MmM}_5$  alloy makes the atomic re-configuration difficult to realize, because long-range diffusion is needed for the growth of a crystalline phase. Therefore, there is only limited growth from the  $\text{MmM}_5$  crystal nuclei formed in the  $\text{MmM}_5$  layer, and, consequently, a nanocrystalline structure is formed.

The fact that the microstructure of the  $\text{MmM}_5$  layer deposited on the top of the Mg layer is the same as that deposited on the Si substrate is because there is an interruption between the deposition of different layers. When the growth of the Mg layer is finished and before the growth of the  $\text{MmM}_5$  layer is started, the temperature of the substrate is decreased during the interruption. Therefore, the growth mechanism of  $\text{MmM}_5$  on the underlying Mg layer is similar to that on the Si substrate. The above results also reveal that the microstructure of the deposited  $\text{MmM}_5$  layer is mainly dependent upon the substrate temperature, regardless of the nature of the substrate such as composition and structure.

#### Microstructure of Mg Layer

Figure 3a,b shows bright field and dark field images taken from a Mg layer with adjacent  $\text{MmM}_5$  layers. Figure 3 shows clearly that the Mg layer is composed of two regions: one is a randomly orientated nanocrystalline region about 50 nm thick from the bottom interface and the other is bundles of parallel columnar Mg crystallites with a width of about 100 nm. Micro-diffraction, dark field imaging, and HRTEM analysis were used to characterize the columnar crystallites in detail. In order to determine the relative orientation between two adjacent columnar crystallites, careful micro-diffraction analysis was employed in the following way. Each of the columnar crystallites, labeled A, B, C, D, and E in Figure 3a, was tilted to the orientation of their [110] direction parallel to the electron beam. Then, the tilting angles of the double tilting specimen holder were recorded to illustrate the orientation difference among the columnar crystallites. Figure 3c–g shows the micro-diffraction patterns corresponding to the Mg columnar crystallites labeled A, B, C, D, and E in Figure 3a. The relative tilting angles are shown in the upper-left corner of each micro-diffraction pattern. The biggest deviation among the above measured columnar crystallites is about  $9^\circ$ , illustrating that the columnar crystallites deviate randomly from each other with a small angle. Figure 3h is a selected area diffraction pattern (SADP) taken from a region containing three columnar crystallites, i.e., A, B, and C. The co-existence of three sets of [110] zone diffraction patterns also indicates a small deviation between columnar crystallites. Trace analysis and HRTEM analysis show that the (001) plane of each columnar crystallite is nearly parallel to the substrate surface, indicating that the columnar crystallites grow along the [001] direction.

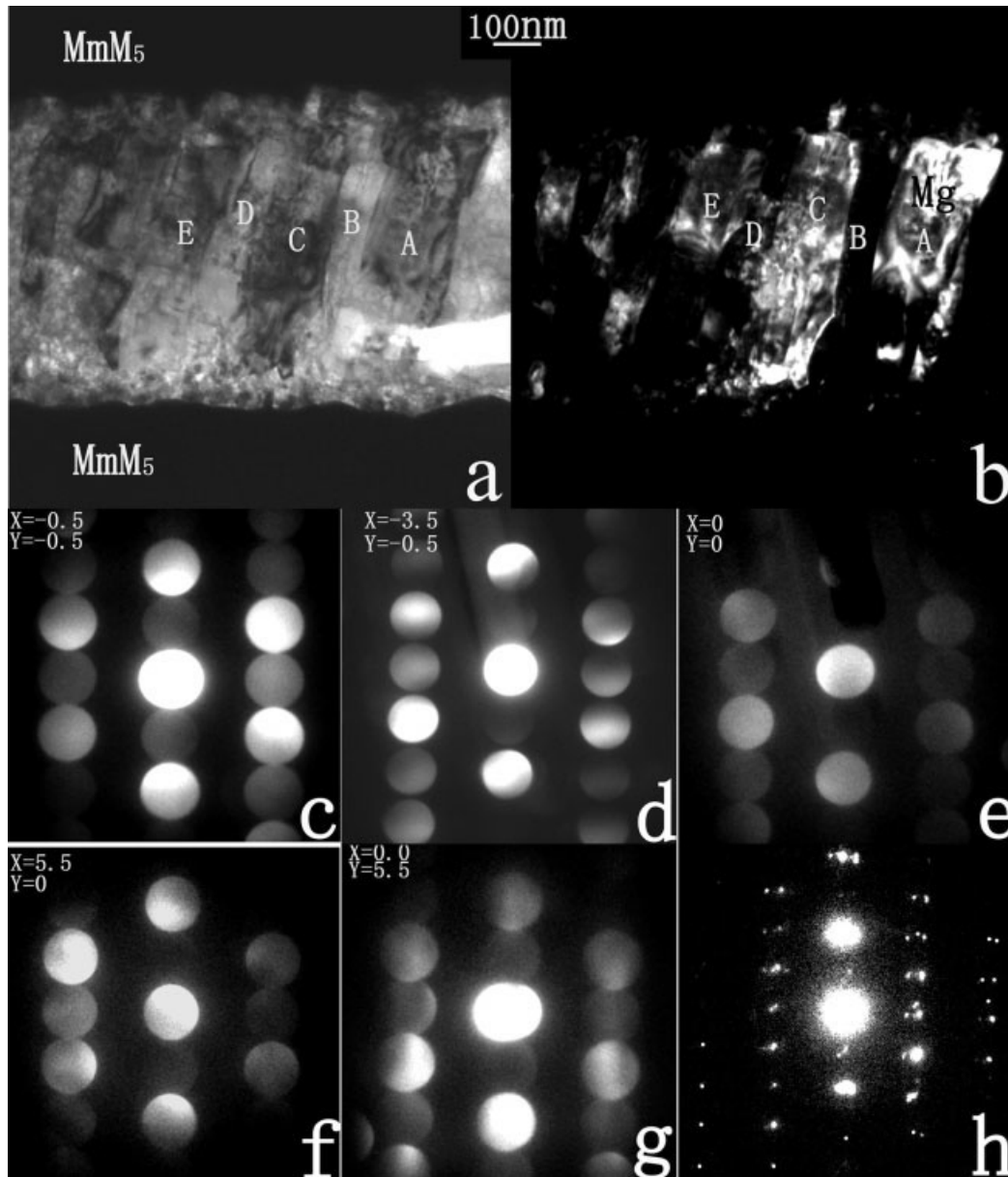


Fig. 3. XTEM images of Mg layer deposited on an underlying  $MmM_5$  layer (a) bright field and (b) dark field. c–g: Micro-beam electron diffraction patterns corresponding to grains A–E, respectively, along [110] direction. h: Composite electron diffraction pattern from grains A, B, and C along the direction close to [110].

This is also in agreement with an X-ray diffraction analysis (Wang et al., 2004).

Figure 4 is an HRTEM image of a Mg layer taken from the region near the underlying  $MmM_5$  layer, where nanocrystallites (as marked by A and B) and columnar crystallites (as marked by C, D, and E) can be seen. It clearly shows that crystallites A and B are randomly orientated, while the [001] directions of columnar crystallites C, D, and E are almost parallel to the growth direction of the deposited film. This morphology enables us to understand the evolution of the growth of the Mg layer. It is noted that (1) similar to the deposition process of the  $MmM_5$  layer, the cooling

rate in the initial deposition stage is rather high, and (2) it is almost impossible for a pure metal to form an amorphous phase. These two facts lead to the formation of Mg crystalline grains with a high nucleation rate in the initial stage of deposition. Therefore, nanocrystalline grains, such as grains A and B, are formed with random orientation in the initial stage of the growth of the Mg layer, and a thin nanocrystalline region of Mg is formed on the top of  $MmM_5$  layer. Once these nanocrystalline grains are formed, further growth of Mg can be considered as in-house growth. The fact that columnar crystallites with (001) planes are parallel to the underlying surface suggests that

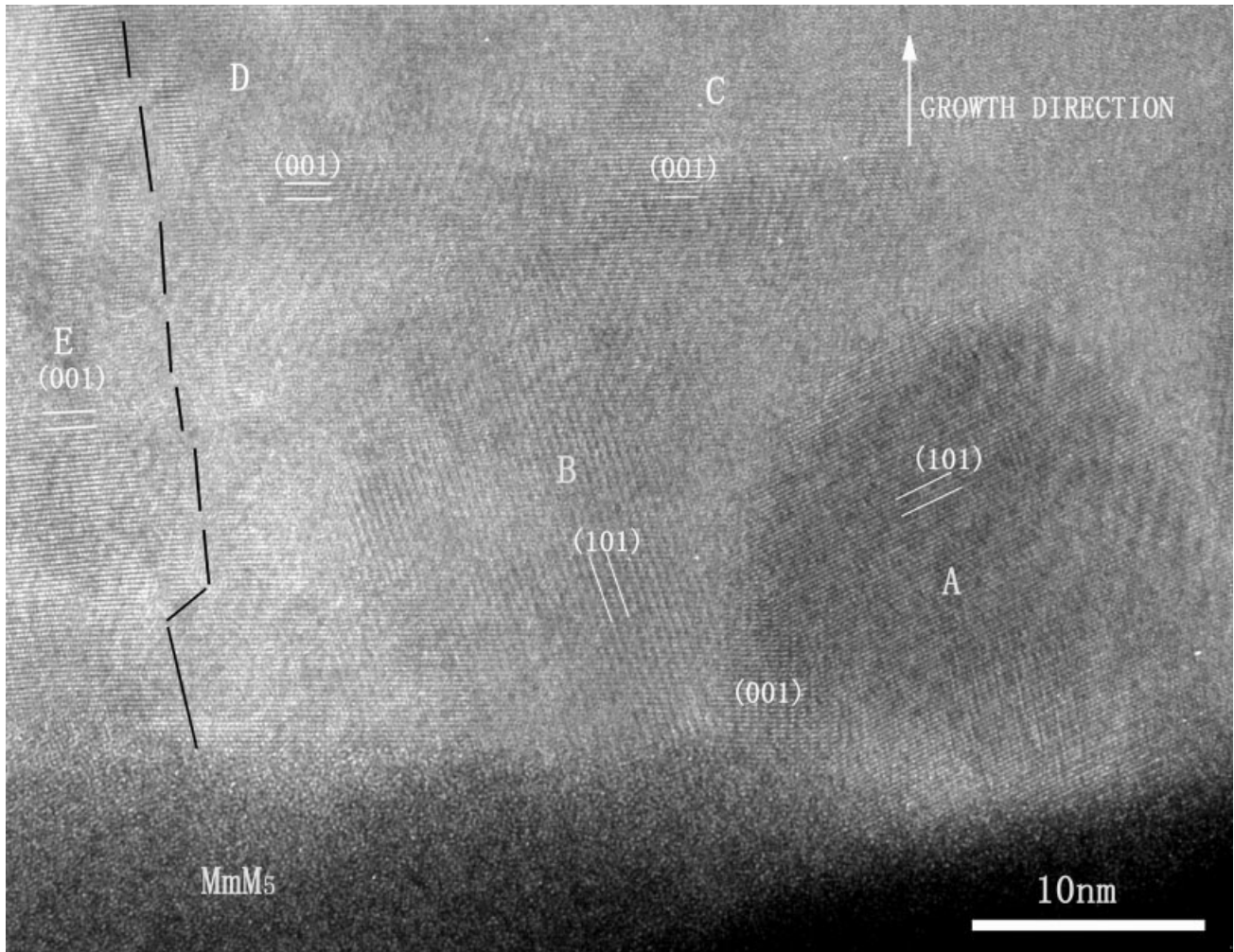


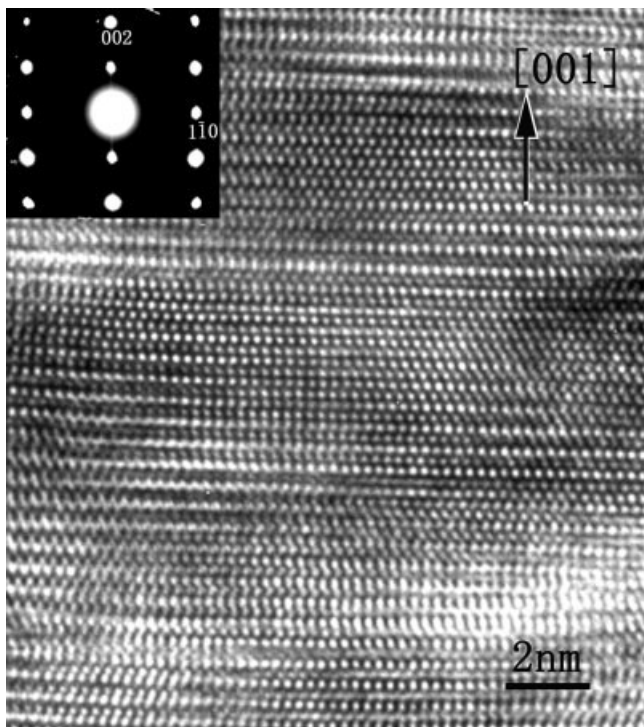
Fig. 4. HREM image of the Mg layer in the region near the underlying  $\text{MmM}_5$  layer showing nanocrystalline and columnar regions.

those nanocrystalline grains with their [001] direction parallel to the growth direction would be preferred nuclei for the further growth of Mg. In fact, the (001) plane in Mg is the close-packed plane, hence is the lowest surface energy plane. For this reason, it is energetically favorable for the growth facet to be on the (001) plane (Fugii et al., 2002; Lee et al., 2003). With further growth, those nanocrystalline grains with their [001] directions parallel to the growth direction should grow fast, while other grains with their [001] directions away from the growth direction experience slow and/or even restricted further growth. The result is predominant growth only of grains with their [001] directions parallel to the growth direction. Consequently, columnar crystallites are formed.

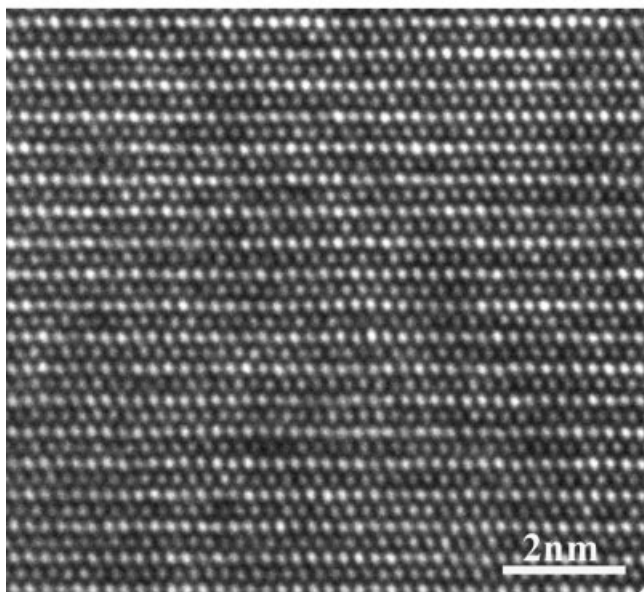
Figure 5a is an HRTEM image of a Mg grain marked as C in Figure 4 with the corresponding SADP inserted in the top-left corner. A significant stress is seen from Figure 5a. First of all, the blurred white/dark background indicates the existence of strain. Also, Figure 5a shows a considerable bending of the crystal lattice. It is well known that, for a hexagonal close packed structure, the stacking sequence along the c

axis is . . . ABABAB . . . In Figure 5a, one may find such an atomic arrangement in some areas, but not in other areas. This also indicates that the deposited films contain a high stress. This is because the existing strain is relieved through a local bending of the thin foil specimen when a thin TEM specimen was prepared, resulting in the imaging condition varying in different areas of the specimen. Figure 5b is an HREM image of columnar Mg crystallites in film annealed at 573K for 30 seconds. The image shows an undistorted structure of the Mg lattice, implying that the strain in the as-deposited film was eliminated after the annealing process.

Although the [001] orientations of columnar crystallites deviate more or less randomly from each other in a range of small angles in most cases, large-angle interface boundaries between columnar crystallites can also be observed occasionally. Two examples for large-angle and small-angle misorientation between adjacent columnar crystallites are shown in Figure 6a and b, respectively. Figure 6a shows two columnar crystallites that grow from the  $\text{MmM}_5$  surface directly with their (001) planes at an angle of about  $20^\circ$ . Figure 6b



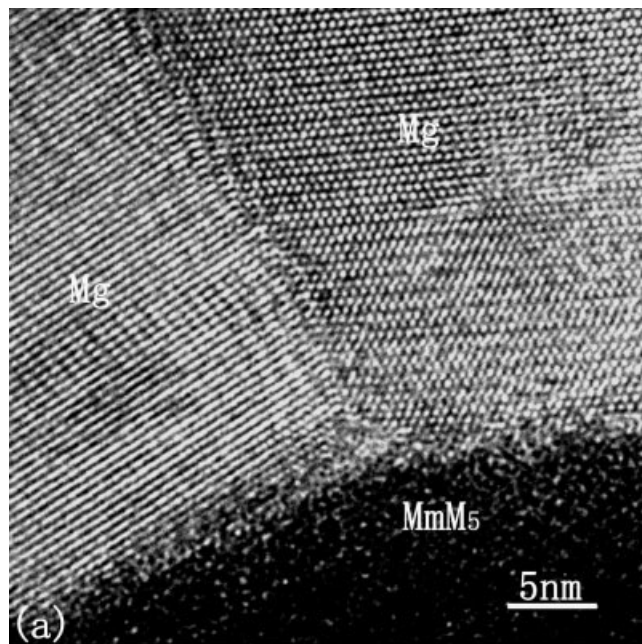
a



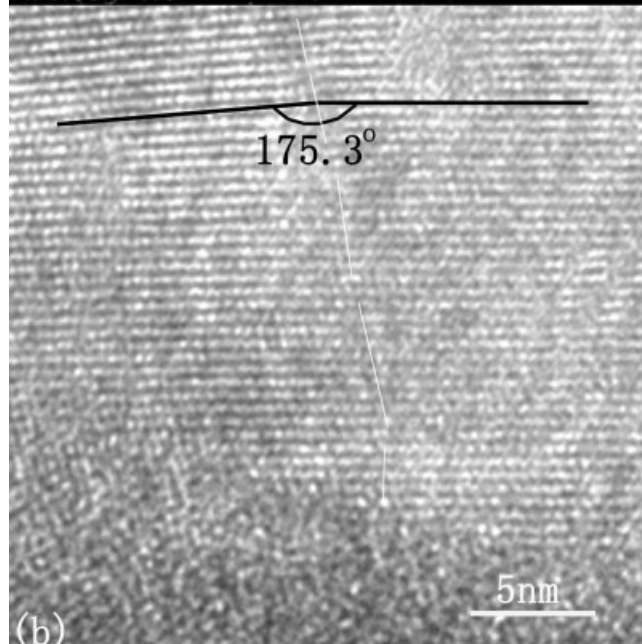
b

Fig. 5. **a:** HREM of a Mg grain along [110] direction showing the distortion of the film. The corresponding SADP is inserted in the upper-left corner in the image. **b:** HREM of a Mg grain along [110] direction in the film annealed at 573K for 30 seconds.

shows two columnar crystallites with the angle between their (001) planes of about  $5^\circ$ . In all the cases observed, the grain boundary is not a symmetric tilted type. Therefore, it is impossible to obtain a clear interface of the two neighboring crystallites while keeping



(a)



(b)

Fig. 6. **a:** Two columnar crystallites with their (001) planes at an angle of  $\sim 20^\circ$ . **b:** Two columnar crystallites with their (001) planes at an angle of  $\sim 5^\circ$ .

the (001) planes of the both crystallites parallel to the incident electron beam.

### SUMMARY

It has been demonstrated that high-quality Mg/MmM<sub>5</sub> multi-layer composite films can be prepared by direct current magnetron sputtering with a well-controlled film thickness and a well-bonded interface between different layers. Apparently, the microstructures of the MmM<sub>5</sub> layer and the Mg layer are different. For the MmM<sub>5</sub> layer, the majority is MmM<sub>5</sub>

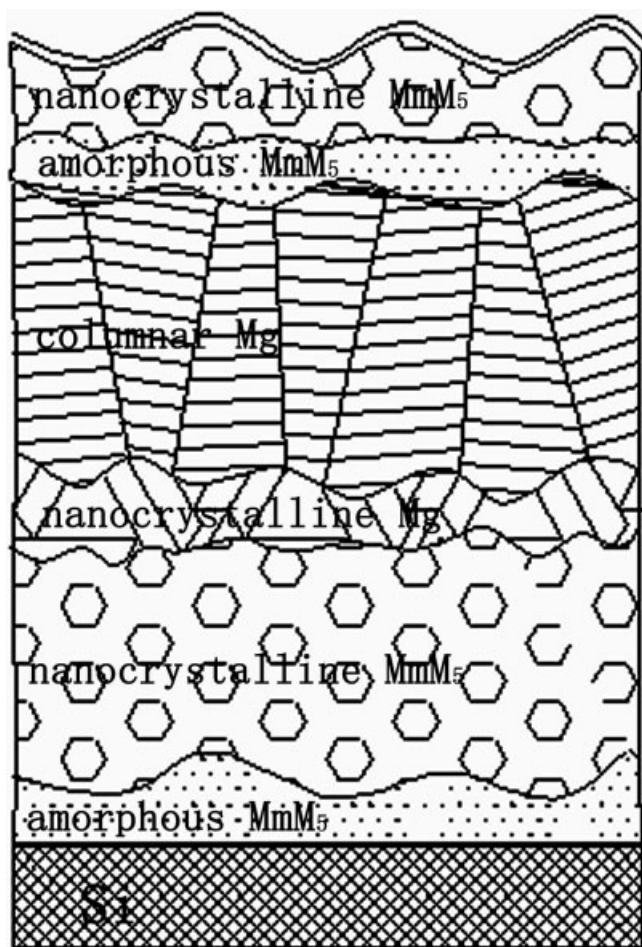


Fig. 7. A schematic illustration showing the microstructure of the multi-layer thin film.

nanocrystallites with a thin amorphous layer about 4 nm thick at the bottom of the layer. For the Mg layer, the majority is columnar crystallites with a thin layer of randomly orientated nanocrystallites about 50 nm thick at the bottom of the layer. Most of columnar crystallites have their [001] directions roughly parallel to the growth direction. All interfaces between different layers are clean without interface phases. The detailed microstructure of the multi-layer film is schematically illustrated in Figure 7. The formation of the film microstructure is mainly dependent on the deposition conditions and the composition of the deposited layer.

## REFERENCES

- Aizawa T, Kuji T, Nakano H. 1999. Synthesis of  $\text{Mg}_2\text{Ni}$  alloy by bulk mechanical alloying. *J Alloys Compounds* 291:248–253.
- Berlouis LEA, Cabrera E, Hall-Barientos E, Hall PJ, Dodd S, Morris S, Imam MA. 2000. A thermal analysis investigation of the hydriding properties of nanocrystalline Mg–Ni based alloys prepared by high energy ball milling. *J Alloys Compounds* 305:82–89.
- Bobet J, Akiba E, Darriet B. 2000a. Effect of substitution of Fe and Ni for Co in the synthesis of  $\text{Mg}_2\text{Co}$  compound using the mechanical alloying method. *J Alloys Compounds* 97:192–198.
- Bobet J, Akiba E, Nakamura Y, Darriet B. 2000b. Study of Mg–M (M=Co, Ni and Fe) mixture elaborated by reactive mechanical alloying–hydrogen sorption properties. *Int J Hydrogen Energy* 25: 987–996.
- Bobet J, Akiba E, Darriet B. 2001. Study of Mg–M (M=Co, Ni –996 and Fe) mixture elaborated by reactive mechanical alloying: hydrogen sorption properties. *Int J Hydrogen Energy* 26:493–501.
- Chen J, Yang H, Xia Y, Kuriyama N, Xu Q, Sakai T. 2002. Hydriding and dehydriding properties of amorphous magnesium–nickel films prepared by a sputtering method. *Chem Mater* 14:2834–2836.
- Choi W, Tanaka T, Miyauchi R, Morikawa T, Inoue H, Iwakura C. 2000. Electrochemical and structural characteristics of  $\text{TiV}_2.1\text{Ni}_0.3$  surface-modified by ball-milling with  $\text{MgNi}$ . *J Alloys Compounds* 299:141–147.
- Cui N, He P, Luo JL. 1999. Magnesium-based hydrogen storage materials modified by mechanical alloying. *Acta Mater* 47:3737–3743.
- Fujii H, Higuchi K, Yamamoto K, Kajioka H, Orimo S, Toiyama K. 2002. Remarkable hydrogen storage, structural and optical properties in multi-layered Pd/Mg thin films. *Mater Transact* 43:2721–2727.
- Fujii H, Orimo S. 2003. Hydrogen storage properties in nano-structured magnesium- and carbon-related materials. *Physica B* 328:77–80.
- Gao Y, Zeng MQ, Li BL, Zhu M. 2003. Solid state reaction and formation of nano-phase composite hydrogen storage alloy by mechanical alloying of  $\text{MmNi}(3.5)(\text{CoMnAl})(1.5)$  and Mg. *J Mater Sci* 38:2499–2504.
- Goo NH, Jeong WT, Lee KS. 2000. Effects of Zr addition on discharge properties of mechanically alloyed  $\text{Mg}_2\text{Ni}$  hydrogen-storage alloy electrode. *Power Sources* 87:118–124.
- Higuchi K, Yamamoto K, Kajioka H, Toiyama K, Honda M, Orimo S, Fujii H. 2002. Remarkable hydrogen storage properties in three-layered Pd/Mg/Pd thin films. *J Alloys Compounds* 526:330–332.
- Hong T, Kim S, Kim Y. 2000. Dehydrogenation properties of nano/amorphous  $\text{Mg}_2\text{NiH}_x$  by hydrogen induced mechanical alloying. *J Alloys Compounds* 312:60–67.
- Huot J, Liang G, Schulz R. 2003. Magnesium-based nanocomposites chemical hydrides. *J Alloys Compounds* 353:L12–L15.
- Imamura H, Sakasai N. 1995. Hydriding characteristics of Mg-based composites prepared using a ball mill. *J Alloys Compounds* 231: 810–814.
- Imamura H, Sakasai N, Kajii Y. 1996. Hydrogen absorption of Mg-based composites prepared by mechanical milling: factors affecting its characteristics. *J Alloys Compounds* 232:218–223.
- Kohno T, Yamamoto M, Kanda M. 1999. Electrochemical properties of mechanically ground  $\text{Mg}_2\text{Ni}$  alloy. *J Alloys Compounds* 643:293–295.
- Lee HY, Goo NH, Jeong WT, Lee KS. 2000. The surface state of nanocrystalline and amorphous  $\text{Mg}_2\text{Ni}$  alloys prepared by mechanical alloying. *J Alloys Compounds* 313:258–262.
- Lee MH, Bae IY, Kim KJ, Moon KM, Oki T. 2003. Formation mechanism of new corrosion resistance magnesium thin films by PVD method. *Surface Coat Technol* 670:169–170.
- Morris S, Dodd SB, Hall PJ, Mackinnon AJ, Berlouis LEA. 1999. The effect of novel processing on hydrogen uptake in FeTi- and magnesium-based alloys. *J Alloys Compounds* 458:293–295.
- Nohara S, Fujita N, Zhang SG. 1998. Electrochemical characteristics of a homogeneous amorphous alloy prepared by ball-milling  $\text{Mg}_2\text{Ni}$  with Ni. *J Alloys Compounds* 267:76–78.
- Orimo S, Fujii H. 2001. Materials science of Mg–Ni-based new hydrides. *Appl Phys A* 72:167–186.
- Paillier J, Dolbec R, Khakani M, Roué L. 2003. Electrochemical behavior of Mg–Ni–Ti thin films grown by pulsed laser deposition. *J Alloys Compounds* 358:126–132.
- Richardson TJ, Farangis B, Slack JL, Nachimuthu P, Perera R, Tamura N, Rubin M. 2003. X-ray absorption spectroscopy of transition metal–magnesium hydride thin films. *J Alloys Compounds* 356: 204–207.
- Wang H, Ouyang LZ, Peng CH, Zeng MQ, Chung CY, Zhu M. 2004.  $\text{MmM}_5/\text{Mg}$  multi-layer hydrogen storage thin films prepared by DC magnetron sputtering. *J Alloys Compounds* 370:L4–L6.
- Yamaura S, Kim H, Kimura H, Inoue A, Arata Y. 2002. Thermal stabilities and discharge capacities of melt-spun Mg–Ni-based amorphous alloys. *J Alloys Compounds* 339:230–235.
- Yang QM, Ciureanu M, Ryan DH. 1998. Composite hydride electrode materials. *Journal of Alloy and Compounds*. *J Alloys Compounds* 274:266–273.
- Zaluska A, Zaluski L, Ström-Olsen JO. 2001. Catalysis and atomic reactions on the nano-scale: a systematic approach to metal hydrides for hydrogen storage. *Appl Phys A* 72:157–165.
- Zhou HW, Kharas BG, Gouma PI. 2003. Microstructure of thick polycrystalline silicon films for MEMS application. *Sensors Actuators A: Physical* 104:1–5.
- Zhu M, Wang ZM, Peng CH, Zeng MQ, Gao Y. 2003. The effect of grain refining on the discharge capacity of  $\text{Mg}_2\text{Ni}/\text{MmNi}_5\text{-x}(\text{CoAlMn})_x$  composite prepared by mechanical alloying. *J Alloys Compounds* 349:284–289.